Influence of muscle-tendon complex geometrical parameters on modeling passive stretch behavior with the Discrete Element Method.

Anthony Roux, Sébastien Laporte, Jennyfer Lecompte, Laure-Lise Gras, Ivan Iordanoff

Journal of Biomechanics

Influence of muscle-tendon complex geometrical parameters on modeling passive stretch behavior with the Discrete Element Method

A. Roux [a,b,*], S. Laporte [a], J. Lecompte [a], L.-L. Gras [a], I. Iordanoff [b]

[a] Arts et Métiers ParisTech, Institut de Biomécanique Humaine Georges Charpak, LBM, 151 bd de l'Hôpital, 75013 Paris, France
[b] Arts et Métiers ParisTech. I2M. Esplanade des Arts et Métiers, 33405 Talence, France

Keywords:
Muscle-tendon complex
Discrete Element Method
Pennation angle
Hyper-elastic behavior

A B S T R A C T

The muscle-tendon complex (MTC) is a multi-scale, anisotropic, non-homogeneous structure. It is composed of fascicles, gathered together in a conjunctive aponeurosis. Fibers are oriented into the MTC with a pennation angle. Many MTC models use the Finite Element Method (FEM) to simulate the behavior of the MTC as a hyper-viscoelastic material. The Discrete Element Method (DEM) could be adapted to model fibrous materials, such as the MTC. DEM could capture the complex behavior of a material with a simple discretization scheme and help in understanding the influence of the orientation of fibers on the MTC's behavior. The aims of this study were to model the MTC in DEM at the macroscopic scale and to obtain the force/displacement curve during a non-destructive passive tensile test. Another aim was to highlight the influence of the geometrical parameters of the MTC on the global mechanical behavior. A geometrical construction of the MTC was done using discrete element linked by springs. Young's modulus values of the MTC's components were retrieved from the literature to model the microscopic stiffness of each spring. Alignment and re-orientation of all of the muscle's fibers with the tensile axis were observed numerically. The hyper-elastic behavior of the MTC was pointed out. The structure's effects, added to the geometrical parameters, highlight the MTC's mechanical behavior. It is also highlighted by the heterogeneity of the strain of the MTC's components. DEM seems to be a promising method to model the hyper-elastic macroscopic behavior of the MTC with simple elastic microscopic elements.

1. Introduction

Tearing of the muscle-tendon complex (MTC) is a common sports-related injury (Bianchi et al., 1998). Muscles are more prone to tear while doing eccentric exercises in which muscle contraction is combined with excessive stretching (Petilon et al., 2005, Bianchi et al., 2006, Chen et al., 2009, Uchiyama et al., 2011). Following a tear of a muscle, functional impairment occurs as the result of the alteration of the MTC's mechanical properties. However, the mechanisms leading to such an injury are still unclear as are the site of mechanical failure and structures involved (Brickson et al., 2011, Butterfield and Herzog, 2006, Pratt et al., 2012). Knowing these mechanisms could provide a rational basis for preventing such injury and/or rehabilitation (Morisawa et al., 1997, Uchiyama et al., 2011). In order to better understand and model tearing of the MTC, a first step is to model and validate the MTC's behavior.

The MTC is a multi-scale, anisotropic, non-homogeneous structure. It is composed of fascicles that are gathered together in a conjunctive aponeurosis (epimysium). The use of computational methods has been used extensively in biomechanics to model the MTC's mechanical behavior. Many models of the MTC use the Finite Element Method (FEM) to simulate the MTC's behavior as an incompressible and hyper-viscoelastic material (Yucesoy et al., 2002), using, for instance, Odgen's law (Bosboom et al., 2001, Gras et al., 2012) or Mooney-Rivlin's law (Weiss et al., 1996, Untaroiu et al., 2005). Most Finite Element models have complex, non-linear mechanical properties and many parameters (Hernandez-Gascon et al., 2013). In Finite Element models, the behavior of the muscle's architecture is described with consitutive laws. These laws can be complex as they also include the complex

* Corresponding author at: Institut de Biomécanique Humaine Georges Charpak (Laboratoire de Biomécanique) Arts et Métiers ParisTech, 151 Boulevard de l'Hôpital, 75013 Paris, France. Tel.: +33 144246364; fax: +33 144246366.
E-mail address: anthony.roux@ensam.eu (A. Roux).

micro-architecture of the muscle. Many authors use this technique to describe the muscle and fibers' behavior (Blemker and Delp, 2005, Tang et al., 2009, Grasa et al., 2011, Böl et al., 2011, 2012). Another interesting approach is to describe the micro architecture with simple constitutive laws as done in the Discrete Element Method. The Discrete Element Method (DEM) (Cundall and Strack, 1979), which is used for modeling granular assemblies or for the manufacturing of composite materials (Fillot et al., 2007, Iliescu et al., 2010), can be adapted to fibrous materials such as the MTC. To the best of our knowledge, this is the first time this method has been applied to the MTC. It allows taking into account the microstructure of the MTC and the influence of its components on its global response. As opposed to FEM, DEM can capture the complex behavior of a material with a simple discretization scheme in terms of concept (Tavarez and Plesha, 2007) and implementation. DEM is also an efficient tool to understand the influence of fibers' orientation on the MTC's behavior or to take into account failure problems (André et al., 2013).

Then, as the first step to model the MTC's tear, the aims of this study were, to model the MTC using DEM, at a macroscopic scale, to reproduce the non-linear force/displacement curve obtained experimentally for the passive muscle behavior during a non-destructive passive tensile test, and to highlight the influence of geometrical parameters of the MTC on the global mechanical behavior during a passive tensile test.

2. Material and methods

2.1. MTC model

2.1.1. Geometrical construction and discrete elements

A set of DEM MTC models based on different muscles' and tendons' geometrical parameters was constructed. This approach allowed us to assess the influence of the muscles' and tendons' lengths, widths, and thicknesses and the influence of the orientation of fibers, as characterized by pennation angles ranging from 0° to 90°. MTC is composed of tendon and muscle, and it includes fibers, a matrix and the epimysium. Tendon is inserted finger-like into the muscle to represent the myotendinous junction (Trotter et al., 1985, Trotter, 2002, Hijikata et al., 1993, Turrina et al., 2013) (Fig. 1). Each discrete element of the tendon is linked to several discrete elements of the muscle: one discrete tendon element is linked to the discrete muscle element situated in front of it, and to the two closest neighboring discrete muscle elements. The same operation is duplicated with the next row. The length and width of the myotendinous junction can also be modified. All these parameters are assumed to be representative parameters of the MTC's geometry.

Discrete elements are created to represent all components. The steps between elements depend on the pennation angle and the maximum number of elements that can be inserted in a fiber in a free-stress position without contact between them.

2.2. Element linking

Links are created between all discrete elements of the same components of the MTC (represented by a set of spherical discrete elements). Some links can also be created between components to model interactions between them, *i.e.*, the myotendinous junction. For instance, muscle's fibers are modeled by a chain of discrete elements linked to each other. The tendon's fibers are composed of fibers with links between them to create sliding. Such fibers have the same architecture as the muscle's fibers. The myotendinous junction (MTJ) is constructed by multi-links between tendon and muscle to respect the finger-like insertion. Links are also created between fibers and the epimysium in order to simulate sliding between these two entities. The extracellular matrix (ECM) is created in all directions by links between fibers.

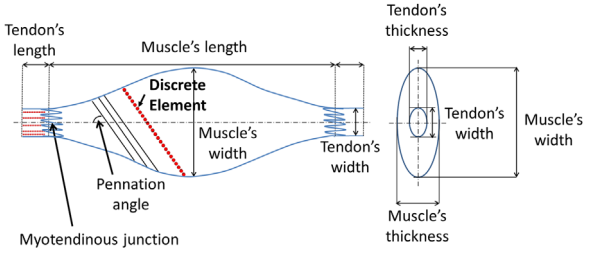

Fig. 1. Front and lateral views of muscle-tendon complex's geometrical parameters.

2.3. Mechanical properties

In the model, springs were used to link the elements to each other. The stiffness of each spring is related to the discrete element's cross-sectional area, the initial length of the springs and Young's Modulus of the anatomical structure (Fig. 2a). Young's modulus values of the muscle's and the tendon's fibers are fixed as the values retrieved from the literature to model the microscopic stiffness of each spring (Table 1). As described by Wang (2006), a specific latency is imposed on the springs that constitute the tendon to model the pre-trigger for the first 2% strain region. This latency corresponds to the "toe" region in which fibers are still crimped. After this region, there will be a linear region with straightened fibers. The epimysium is an extension of the tendon, so it is composed of the same material as the tendon. The Young's modulus of the epimysium used in the model is therefore the same as the tendon's Young's modulus (Maganaris and Paul, 2000, Teran et al., 2005, Azizi et al., 2009). However, since the epimysium is a fascia of the MTC, sections of the epimysium's discrete elements are smaller than the MTC's other components in order to obtain a thin fascia for the MTC. The myotendinous junction's Young's modulus is supposed to have a value that is intermediate between Young's moduli of the muscle's fibers and the tendon.

ECM is supposed to be "fibers" of matrix between the muscle's fibers, and it has the same geometrical properties as the MTC's other components. The ECM's mechanical behavior was modified to model the possible contact between two fibers. In compression, if the length of the ECM's spring was smaller than the initial step between the extremities of two discrete elements (Δs), and the ECM's stiffness was equal to the fiber's stiffness (Fig. 2b). Because of the lack of values in the literature, several values of Young's modulus were tested in order to obtain the same aspect as the experimental curves (Gras et al., 2012). Thus, the value for the ECM's Young's modulus was chosen as 0.1 MPa.

3. Analysis of the influence of geometrical parameters

3.1. Design of experiments

A complete design of experiments was prepared to determine the geometrical parameters that affect the MTC's mechanical behavior and to identify existing interactions between them. The mean value of each geometrical parameter with a variation of more or less one standard deviation was chosen to construct the MTCs with due consideration of data from the literature (Gras et al., 2012). The widths and thicknesses of the muscle and the tendon were chosen to be equals to each other. Five angles were chosen to better characterize the influence of the pennation angle, in agreement with the literature (Kawakami et al., 2006). Table 2 provides a summary of all geometrical parameters and tested values. This complete design of experiments represents 405 possibilities of MTC.

3.2. Tensile test simulation and boundary conditions

GranOO software (Granular Object Oriented, www.granoo.org, Mechanics Institute of Bordeaux (I2M)) was used to model MTC and to simulate the tensile tests. First the geometry with links is created. The mechanical properties are then associated to each spring.

In the tensile tests, the lower extremity of the MTC was fixed, and the upper extremity was subjected to a linear displacement with a maximum displacement of 20 mm (strain *c.a.* 10%) with a tensile test speed of 1 mm/s. Visualization of the simulation and data (force, displacement, position) are also obtained.

3.3. Identified parameters

The four studied parameters are listed below:

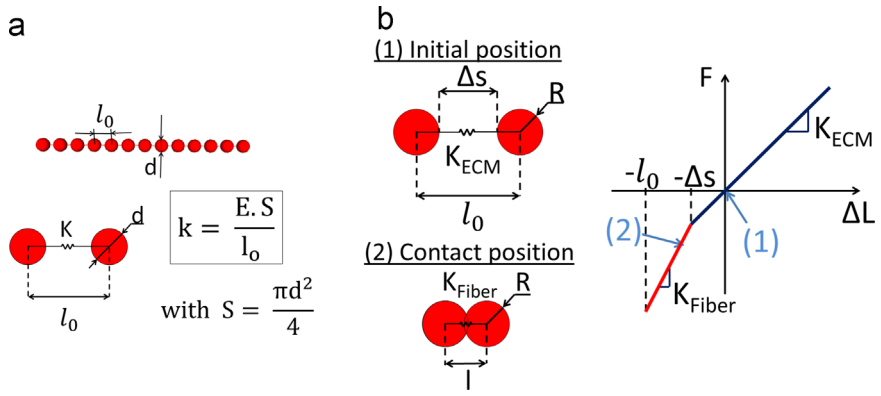

Fig. 2. (a) Relationship between Young's modulus (E) and stiffness (k) for muscle's fiber (l_o=spring's initial length and d=fiber's diameter); (b) Extracellular Matrix's (ECM) stiffness during the tensile and compression tests (R=Discrete element's radius, l=spring's length, ΔL=spring's lengthening, and Δs=initial length between two discrete elements).

Table 1
Young's modulus of muscle-tendon complex's components.

MTC's components	Young's modulus (MPa)	Reference
Tendon's fiber/epimysium	800	Matscheke et al. (2013)
Muscle's fiber	0.03744	Regev et al. (2011)
Myotendinous junction	400	–
ExtraCellular matrix	0.1	–

Table 2
Geometrical parameters of the muscle-tendon complex, and their levels.

Parameters	Level 1	Level 2	Level 3	Level 4	Level 5
Pennation angle (°)	10	15	20	25	30
Muscle's length (mm)	116	134	149	–	–
Muscle's width (mm)	11.0	12.1	13.3	–	–
Tendon's length (mm)	11.6	13.4	14.9	–	–
Tendon's width (mm)	5.5	6.7	8.0	–	–

- Variation of the volume of the MTC based on the calculation of the volume of the external sheath
- σ_{ing}=Force/S_0 (S_0=initial cross-sectional area of the middle of the MTC, where S_0=π*(muscle's width/2)²) (the cross sectional area is circular and the diameter is equal to muscle's width) for ε_{ing}=10% with ε_{ing}=Displacement/L_0 (L_0=MTC's initial length=(muscle's initial length)+2*(tendon's initial length))
- Variation of the pennation angle to study the evolution of the MTC's central fibers

- Force/displacement curves were fitted with a global hyper-elastic law. Parameters μ and α for the identification of the hyper-elastic constitutive law (Ogden's incompressive law (Ogden, 1997)) used by Gras et al. (2012): $F_{Hyper} = \frac{2\mu}{\alpha} s_0 \left(\lambda 1^{\alpha} - \lambda 1^{\alpha/2}\right).\lambda 1^{-1}$ with $\lambda_1 = 1 + \frac{D}{L_0}$ with D=MTC's displacement.

3.4. Data analysis

A two-way ANOVA was used to evaluate the effects of the geometrical parameters on the mechanical properties. Post-hoc Tukey comparisons were used as follow-up to the significant ANOVA results. Significance was set at $p < 0.05$ for all statistical comparisons.

4. Results

All of the DEM models of MTC were created based on the geometrical parameters from the design of experiments (Fig. 3).

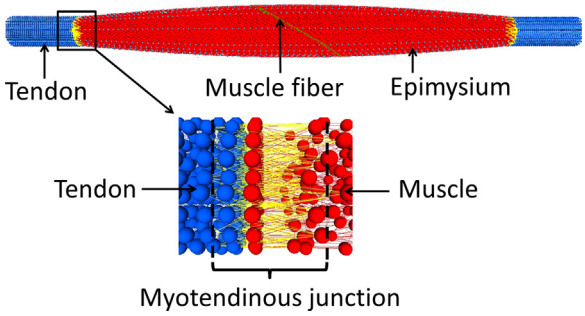

Fig. 3. Muscle-tendon complex's geometry with the Discrete Element Method with an expanded view of the myotendinous junction (springs of epimysium are temporarily hidden for a better view).

All of the models were tested numerically in passive tensile tests. Fig. 4a shows six kinds of force/displacement curves. Efforts ranging between 10 and 40 N were required to obtain the maximum displacement for the simulations. One simulation takes 1h30 (CPU: 1596 MHz, Intel Xeon 3.33 GHz) for a model with 5294 discrete elements and 33420 springs with a discrete element's radius of 0.33275 mm.

The variation of the MTC's volume was estimated during all simulations, and all variations were less than 3%.

Values of σ_{ing} ranged from 11.5 to 88.4 MPa (48.3 ± 15.5 MPa, mean ± SD). The analysis of variance showed that muscle width (MW), tendon width (TW), and pennation angle affected σ_{ing} for ε_{ing}=10%. The higher were TW and pennation angle, the higher was σ_{ing}; the effect was the opposite for MW (Fig. 5a and b).

The pennation angle decreased during the tensile tests in the range of 6–10° (Fig. 4b). The variation of the pennation angle between its initial value and its value at 13% of the muscle's strain was linked to pennation angles with values between 6.7° and 10.7° (Fig. 5c).

For the hyper-elastic constitutive law, the values of μ ranged from 15.7 to 174 kPa (82 ± 32 kPa). MW, TW, and pennation angle affected μ. An increase of TW or pennation angle (or a decrease of MW) caused an increase of μ (Fig. 6a and b). The values of α ranged from 15.2 to 25.6 (20.0 ± 1.9). Its variation was linked to MW (for the increases) and to TW (for the decreases) (Fig. 6c).

5. Discussion

A geometrical construction of the MTC is done using discrete elements linked with springs. During the numerical tensile tests, it was observed that all of the muscle's fibers were reoriented and

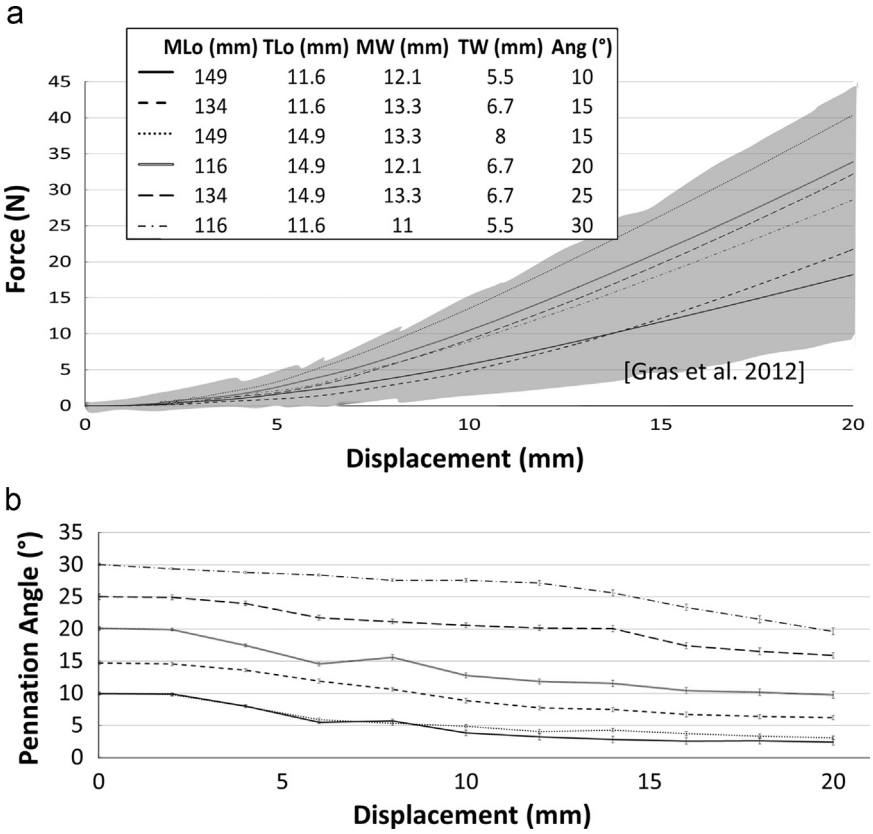

Fig. 4. Examples for different Muscle Lengths (MLo), Tendon Lengths (TLo), Muscle Widths (MW), Tendon Widths (TW) and Pennation Angles (Ang): (a) force/displacement curves compared with experimental results from (Gras et al., 2012); (b) variation of the pennation angle during the tensile tests.

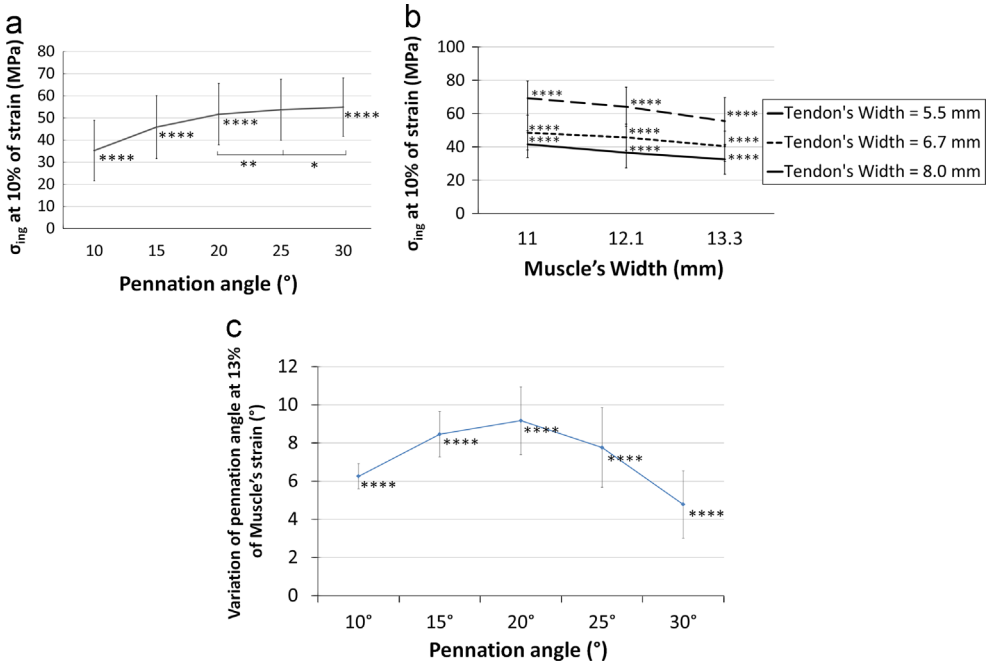

Fig. 5. (a) Influence of Pennation Angle on σ_{ing} for 10% of strain; (b) Cross-influence of Muscle's Width x Tendon's Width on σ_{ing} for 10% of strain; (c) Evolution of the pennation angle's variation between 0% and 13% of muscle's strain, for different values of pennation angle; * for significant correlation. *i.e.* * $p < 0.05$, ** $p < 0.01$, *** $p < 0.001$, **** $p < 0.0001$.

aligned with the tensile axis. The hyper-elastic behavior of the stretching MTC was in agreement with *in vitro* data. Structure effects, added to the geometrical parameters, highlighted the mechanical behavior of the MTC in the tensile test.

The very small variation of volume confirmed the hypothesis that MTC is considered to be a quasi-incompressible material (Teran et al., 2005, Yucesoy et al., 2002, Untaroiu et al., 2005, Behr et al., 2006).

Geometry had a significant effect on the MTC's mechanical behavior. Gras et al. (2012) highlighted the effects of the geometrical parameters on the compressive response of dogs' muscles. In the present study, σ_{ing} depended on MW, TW, and pennation

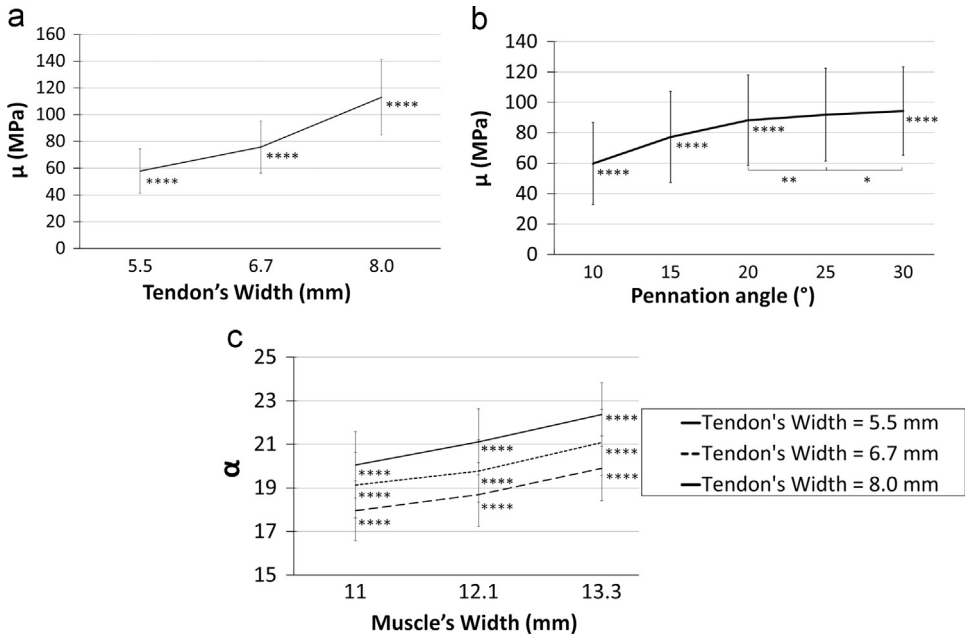

Fig. 6. (a) Effect of Tendon's Width on μ (parameter of the hyper-elastic constitutive law); (b) Effect of Pennation Angle on μ; (c) Cross-effects of Muscle's Width x Tendon's Width on α (parameter of the hyper-elastic constitutive law); * for significant correlation. *i.e.* * $p < 0.05$, ** $p < 0.01$, *** $p < 0.001$, **** $p < 0.0001$.

angle, and it decreased when the MTC's cross-sectional area increased (when MW increased) because the same force was distributed over a larger cross-sectional area. The cross-sectional area of the tendon increased (TW increased), which increased the number of fibers, thereby increasing force required to deform the structure (equivalent to an increase of σ_{ing}). Fig. 5b shows the cross-effect of MW and TW. The third parameter that affected σ_{ing} was the pennation angle; the force required to realign the fibers in the tensile axis increased when more and more fibers tended to be oriented (high pennation angle). Indeed, pennate muscles are more resistant since they have more fibers, and, since these fibers are highly oriented, the force applied to them is lower (Kawakami et al., 2006).

When the muscle's cross-sectional area increases, there is a tendency for the stress to decrease. In fact, a tendon and a muscle can be modeled by two springs in series, with an equivalent stiffness of $k_{eq} = \frac{k_m.k_t}{k_m+k_t}$ where, k_m is the muscle's stiffness, and k_t is the tendon's stiffness.

Equivalent force is $F_{eq} = k_{eq}\Delta L$, and engineering stress (σ_{ing}) is proportional to $\frac{F}{D_m^2}$, where D_m is the diameter of the center of the muscle. The muscle's stiffness is also dependent on the muscle's geometry. Indeed, k_m is proportional to the product, $k_{fm}.D_m^2$, where k_{fm} is the stiffness of the muscle's fiber. Thus, engineering stress is proportional to $\frac{k_{fm}.k_t}{k_{fm}D_m^2+k_t}$. Therefore, if the diameter of the center of the muscle increases (linked to the central cross-sectional area), the engineering stress decreases.

Following the same steps for the tendon, the engineering stress can be found to be proportional to $\frac{1}{D_m^2}.\frac{k_m.k_{tf}}{k_m/D_t^2+k_{tf}}$. For a fixed muscle's cross-sectional area (D_m fixed), if the tendon's cross-sectional area increases (D_t increases), then the engineering stress (σ_{ing}) increases.

The pennation angle decreased during the tensile test, which was in agreement with the literature. Indeed, during passive stretching of a muscle, the pennation angle decreases to the range of approximately 3–7° (Morse et al., 2008, Abellaneda et al., 2009, Zhao et al., 2011). As for composite materials, the values of the pennation angle affected the results of the tensile simulations (Ladevèze et al., 2005, 2012). In pennation angle/displacement curves, two parts can be highlighted. In the first part (until the first

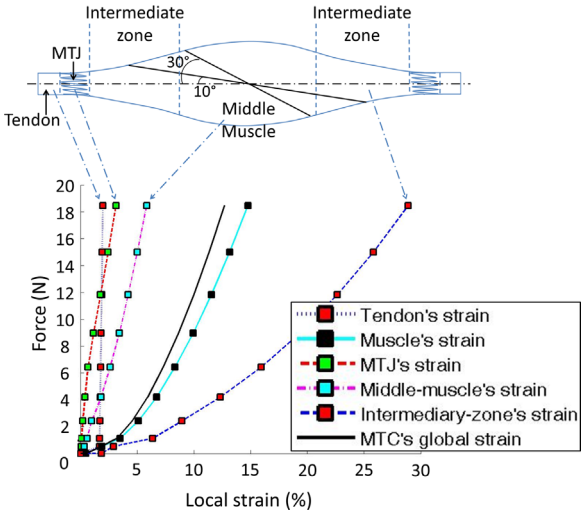

Fig. 7. Force vs. local strain for a muscle-tendon complex (MTC) with Muscle's Length = 134 mm, Tendon's Length = 13.4 mm, Muscle's Width = 12.1 mm, Tendon's Width = 5.5 mm and Pennation Angle = 15°; (MTJ = Muscle-Tendon Junction).

two millimeters), the pennation angle does not vary; this is due to, the initial stretching of the MTC's tendinous parts during the tensile test. Then, in the second part (displacement greater than two millimeters), the variation of the pennation angle is quasi-linear due to the orientation of MTC's fibers with respect to axis of the tensile test. The high variation of the pennation angle between its initial value and its value at 13% of the muscle's strain is linked to the strain of the components that make up the MTC (Fig. 5c). In fact, during the tensile tests, the area of the middle muscle underwent lower strain than the intermediate areas (between MTJ and the area of the middle muscle), which are subject to high, non-linear variations (Fig. 7).

This variation of the pennation angle was also linked to the muscle's form; the more bulging the MTC is (*i.e.* the higher the MW/TW ratio is), the more strained those intermediate areas become. This strain's heterogeneity during tensile test has already been shown in *in vivo* studies (Maganaris et al., 2001, Blazevich

et al., 2006). For pennation angles less than 20°, the central fibers are long and located in intermediate areas, therefore their strain during the tensile test will be higher than when the pennation angle are greater than 20°. This is because, the fibers are shorter, more inclined, and located in the middle-muscle's area where variations of strain are minimal.

The simulations results were in agreement with the experimental data obtained from the SCM muscle within an order of magnitude (Gras et al., 2012). However, because of the lack of knowledge about mechanical properties of the ECM and the myotendinous junction, some hypotheses have been proposed regarding the mechanical behaviors of these components in order to obtain a reasonable fit between the experimental and numerical curves. For example, Young's modulus for the patellar tendon (Matschke et al., 2013) was used, but it cannot be applied directly to SCM's tendon. MTC was created with a simple geometry, with the fibers oriented correctly. Results have to be qualified compared to real studied geometry and geometry's simplifications of our model. In real muscles, the fibers are not oriented perfectly in the direction of pennation angle and then an organization of the fibers occurs during a tensile test (Clemmer et al., 2010). Therefore, a random arrangement of fibers is created to prevent them from being organized perfectly in the muscle. Also, springs are used in the model because their bending rigidity better represents the behavior of the fibers. The mechanical behavior of the MTC is described as finite element models of muscles do (Bosboom et al., 2001, Blemker et al., 2005, Behr et al., 2006, Laville et al., 2009), but with a simple geometry at the microscopic scale, that makes it possible to follow a fiber's behavior easily during a solicitation.

The aspect of the curve can be identified as a non-linear and hyper-elastic behavior for the MTC (Martins et al., 1998, Johansson et al., 2000, Breuls et al., 2003, Blemker and Delp, 2006) and then as a quasi-linear behavior (corresponding to the alignment of the fibers with the axis of the MTC). The non-linear aspect of the curves was in agreement with studies on rabbits (Lin et al., 1999, Morrow et al., 2010), and on mice (Anderson et al., 2002).

Regarding the hyper-elastic constitutive law, its parameters were affected by geometrical parameters. Indeed, μ and α parameters are linked directly to the geometrical parameters of the MTC, *i.e.*, pennation angle, tendon's global stiffness (related to TW), and the size and number of fibers (related to MW). The first model's parameter, μ, is characteristic of the initial slope of the force/displacement curve. The higher μ is, the stiffer the structure is at the beginning of the tensile test. The higher the pennation angles are, the higher μ is; therefore the structure is stiffer (Fig. 6a and b). This is linked to the stiffness of the extracellular matrix, which has a significant effect when the structure is oriented, as explained earlier for the engineering stress. Furthermore, an increase of TW results in an increase of the tendon's global stiffness, which leads to an increase of the MTC's stiffness. Thus, the force will be higher for small displacement, *i.e.*, the parameter μ increases. The second model's parameter, α, is characteristic of the curvature and the hyper-elastic behavior of the curve, and α increases when MW increases or TW decreases (Fig. 6c). The MW/TW ratio, which describes the MTC's form (bulging or straight), is linked to the variation of α. So, for quasi-straight MTC (low MW/TW ratio), intermediate areas (between MTJ and the area of the middle muscle) have constant widths, and their strains are low, inducing a low variation of α, as shown in previous results of the pennation angle (Fig. 5c). For bulging, intermediate areas (ratio MW/TW high), the strain is higher, reflecting their non-linear behavior and inducing an increase in α.

The order of magnitude of α (15.2–25.6, 20 ± 1.9) was the same as reported in the literature. Bosboom et al. (2001) used Ogden's (Ogden, 1997) constitutive law to describe the behavior of a rat's muscle during compression tests. The value of α_{Ogden} in their study (21.4, on average) was equivalent to values of α in the current study. Concerning μ (15.7 to 174 kPa, 82.3 ± 31.8 kPa), Bosboom et al. (2001) used a modulus μ_{Ogden} (15.6 kPa, on average) which is linked to the parameter μ by the relationship $\mu = \mu_{Ogden} \cdot \alpha_{Ogden}/2$. Thus, in compression tests of the rat's muscle, μ was equal to 157 kPa, on average. This value is close to the value identified in the current study, but it was obtained in a compression test. Compared to Gras et al.'s (2012) values, α has the same order of magnitude (16.9–52), and the values of μ in this study were a little higher than those from Gras et al.'s (2012) study (4–98 kPa, 45.7 ± 32.4 kPa), but they had the same order of magnitude.

The results were affected by three main parameters (MW, TW, and pennation angle). These three parameters can properly define MTC's geometry and give a correct overview of all possible responses to a tensile test of the MTC. However, these parameters are linked together because of their dependence on the size and number of the MTC's fibers.

6. Conclusions

The DEM seems to be a promising method for modeling the MTC. The shape of numerical curve was in agreement with the curves obtained experimentally, confirming the possibility of modeling the non-linear, hyper-elastic macroscopic response of a muscle with simple, linear, elastic, microscopic elements. The MTC's behavior seems to result from a geometric effect linked to the reorganization of the fibers in the structure, *i.e.*, the widths of the muscle and tendon and the pennation angle. The model that was developed can account for the effect of fibers, and it allows the identification of two main effects that would be very complex to assass with standard techniques, such as FEM: (1) the influence of fibers' reorientation on mechanical response during the passive tensile test and, (2) the heterogeneous response of the MTC as a function of the pennation angle.

The next step will be to study the stress inside a cross-sectional area of muscle and tendon during the tensile test. This will help to detect where the MTC's rupture is most likely to occur. The muscle activation will be implemented into a spring model, thanks to a force/length law for the muscle's fibers, in order to model an eccentric contraction. All these different parts will then be combined to model the total tear of the MTC.

Conflict of interest statement

The authors have no conflicts of interest to declare.

References

Abellaneda, S., Guissard, N., Duchateau, J., 2009. The relative lengthening of the myotendinous structures in the medial gastrocnemius during passive stretching differs among individuals. J. Appl. Physiol. 106, 169–177.

Anderson, J., Li, Z., Goubel, F., 2002. Models of skeletal muscle to explain the increase in passive stiffness in desmin knockout muscle. J. Biomech. 35, 1315–1324.

André, D., Jebahi, M., Iordanoff, I., Charles, J., Néauport, J., 2013. Using the discrete element method to simulate brittle fracture in the indentation of a silica glass with a blunt indenter. Comput. Methods Appl. Mech. Eng. 265, 136–147.

Azizi, E., Halenda, G.M., Roberts, T.J., 2009. Mechanical properties of the gastrocnemius aponeurosis in wild turkeys. Integr. Comp. Biol. 49, 51–58.

Behr, M., Arnoux, P.-J., Serre, T., Thollon, L., Brunet, C., 2006. Tonic finite element model of the lower limb. J. Biomech. Eng. 128, 223–228.

Bianchi, S., Martinoli, C., Abdelwahab, I.F., Derchi, L.E., Damiani, S., 1998. Sonographic evaluation of tears of the gastrocnemius medial head ("tennis leg"). J. Ultrasound Med. 17, 157–162.

Bianchi, S., Poletti, P.-A., Martinoli, C., Abdelwahab, I.F., 2006. Ultrasound appearance of tendon tears. Part 2: lower extremity and myotendinous tears. Skelet. Radiol. 35, 63–77.

Blazevich, A., Nicholas, G., Shi, Z., 2006. Intra- and intermuscular variation in human quadriceps femoris architecture assessed in vivo. J. Anat. 209, 289–310.

Blemker, S.S., Delp, S.L., 2005. Three-dimensional representation of complex muscle architectures and geometries. Ann. Biomed. Eng. 33, 661–673.

Blemker, S.S., Delp, S.L., 2006. Rectus femoris and vastus intermedius fiber excursions predicted by three-dimensional muscle models. J. Biomech. 39, 1383–1391.

Böl, M., Weikert, R., Weichert, C., 2011. A coupled electromechanical model for the excitation-dependent contraction of skeletal muscle. J. Mech. Behav. Biomed. Mater. 4, 1299–1310.

Böl, M., Kruse, R., Ehret, A.E., Leichsenring, K., Siebert, T., 2012. Compressive properties of passive skeletal muscle-the impact of precise sample geometry on parameter identification in inverse finite element analysis. J. Biomech. 45, 2673–2679.

Bosboom, E.M., Hesselink, M.K., Oomens, C.W., Bouten, C.V., Drost, M.R., Baaijens, F. P., 2001. Passive transverse mechanical properties of skeletal muscle under in vivo compression. J. Biomech. 34, 1365–1368.

Breuls, R.G., Bouten, C.V., Oomens, C.W., Bader, D.L., Baaijens, F.P., 2003. A theoretical analysis of damage evolution in skeletal muscle tissue with reference to pressure ulcer development. J. Biomech. Eng. 125, 902–909.

Brickson, S., Hollander, J., Corr, D.T., Ji, L.L., Best, T.M., 2011. Oxidant production and immune response after stretch injury in skeletal muscle. Med. Sci. Sport. Exerc. 33, 2010–2015.

Butterfield, T.A., Herzog, W., 2006. Effect of altering starting length and activation timing of muscle on fiber train and muscle damage. J. Appl. Physiol. 100 (5), 1489–1498.

Chen, C.P., Tang, S.F., Hsu, C.-C., Chen, R.L., Hsu, R.C., Wu, C.-W., Chen, M.J., 2009. A novel approach to sonographic examination in a patient with a calf muscle tear: a case report. J. Med. Case Rep. 3, 7291.

Clemmer, J., Liao, J., Davis, D., Horstemeyer, M.F., Williams, L.N., 2010. A mechanistic study for strain rate sensitivity of rabbit patellar tendon. J. Biomech. 43, 2785–2791.

Cundall, P.A., Strack, O.D.L, 1979. A discrete numerical model for granular assemblies. Géotechnique 29, 47–65.

Fillot, N., Iordanoff, I., Berthier, Y., 2007. Modelling third body flows with a discrete element method—a tool for understanding wear with adhesi ve particles. Tribol. Int. 40, 973–981.

Gras, L.-L., Mitton, D., Crevier-Denoix, N., Laporte, S., 2012. The non-linear response of a muscle in transverse compression: assessment of geometry influence using a finite element model. Comput. Methods Biomech. Biomed. Eng. 15 (1), 13–21.

Gras, L.-L., Mitton, D., Viot, P., Laporte, S., 2012. Hyper-elastic properties of the human sternocleidomastoideus muscle in tension. J. Mech. Behav. Biomed. Mater. 15, 131–140.

Grasa, J., Ramirez, A., Osta, R., Muñoz, M.J., Soteras, F., Calvo, B., 2011. A 3D active-passive numerical skeletal muscle model incorporating initial tissue strains. Validation with experimental results on rat tibialis anterior muscle. Biomech. Model. Mechanobiol. 10, 779–787.

Hernandez-Gascon, B., Grasa, J., Calvo, B., Rodriguez, J.F., 2013. A 3D electromechanical continuum model for simulating skeletal muscle contraction. J. Theor. Biol. 335, 108–118.

Hijikata, T., Wakisaka, H., Niida, S., 1993. Functional combination of tapering profiles and overlapping arrangements in nonspanning skeletal muscle fibers terminating intrafascicularly. Anat. Rec. 236, 602–610.

Iliescu, D., Gehin, D., Iordanoff, I., Girot, F., Gutiérrez, M., 2010. A discrete element method for the simulation of CFRP cutting. Compos. Sci. Technol. 70, 73–80.

Johansson, T., Meier, P., Blickhan, R., 2000. A finite-element model for the mechanical analysis of skeletal muscles. J. Theor. Biol. 206, 131–149.

Kawakami, Y., Abe, T., Kanehisa, H., Fukunaga, T., 2006. Human skeletal muscle size and architecture: variability and interdependence. Am. J. Hum. Biol. 18, 845–848.

Ladevèze, P., Daghia, F., Abisset, E., LeMauff, C., 2012. A micromechanics-based interface mesomodel for virtual testing of laminated composites. Adv. Model. Simul. Eng. Sci. 1, 7.

Ladevèze, P., Trovalet, M., Lubineau, G., 2005. Multiscale Modelling of Damage and Fracture Processes in Composite Materials. Section Multiscale Computational Damage Modelling of Laminate Composites. Springer-Verlag, p. 309.

Laville, A., Laporte, S., Skalli, W., 2009. Parametric and subject-specific finite element modelling of the lower cervical spine. Influence of geometrical parameters on the motion patterns. J. Biomech. 42, 1409–1415.

Lin, R., Chang, G., Chang, L., 1999. Biomechanical properties of muscle-tendon unit under high-speed passive stretch. Clin. Biomech. (Bristol, Avon) 14, 412–417.

Maganaris, C.N., Paul, J.P., 2000. In vivo human tendinous tissue stretch upon maximum muscle force generation. J. Biomech. 33, 1453–1459.

Maganaris, C.N., Kawakami, Y., Fukunaga, T., 2001. Changes in aponeurotic dimensions upon muscle shortening: in vivo observations in man. J. Anat. 199, 449–456.

Martins, J., Pires, E., Salvado, R., Dinis, P., 1998. A numerical model of passive and active behavior of skeletal muscles. Comput. Methods Appl. Mech. Eng. 151, 419–433.

Matschke, V., Jones, J.G., Lemmey, A.B., Maddison, P.J., Thom, J.M., 2013. Patellar tendon properties and lower limb function in rheumatoid arthritis and ankylosing spondylitis versus healthy controls: a cross-sectional study. Sci. World J., 514743.

Morisawa, K., Yamashita, K., Asami, A., Nishikawa, H., Watanabe, H., 1997. Spontaneous rupture of the deltoid muscle associated with massive tearing of the rotator cuff. J. Shoulder Elb. Surg. 6, 556–558.

Morrow, D.A., Haut, T.L., Odegard, G.M., Kaufman, K.R., 2010. Transversely isotropic tensile material properties of skeletal muscle tissue. J. Mech. Behav. Biomed. Mater. 3, 124–129.

Morse, C.I., Degens, H., Seynnes, O.R., Maganaris, C.N., Jones, D.A., 2008. The acute effect of stretching on the passive stiffness of the human gastrocnemius muscle tendon unit. J. Physiol. 586, 97–106.

Ogden, R.W., 1997. Non-linear Elastic Deformations. Dover Publications Inc (D. P. Inc., Éd.).

Petilon, J., Ellingson, C., Sekiya, J., 2005. Pectoralis major muscle ruptures. Oper. Tech. Sport. Med. 13, 162–168.

Pratt, S.J.P., Lawlor, M.W., Shah, S.B., Lovering, R.M., 2012. An in vivo rodent model of contraction-induced injury in the quadriceps muscle. Injury 43 (6), 788–793.

Regev, G.J., Kim, C.W., Tomiya, A., Lee, Y.P., Ghofrani, H., Garfin, S.R., Lieber, R.L., Ward, S.R., 2011. Psoas muscle architectural design, in vivo sarcomere length range, and passive tensile properties support its role as a lumbar spine stabilizer. Spine (Phila. Pa. 1976) 36, E1666–E1674.

Tang, C.Y., Zhang, G., Tsui, C.P., 2009. A 3D skeletal muscle model coupled with active contraction of muscle fibres and hyperelastic nehaviour. J. Biomech. 42, 865–872.

Tavarez, F.A., Plesha, M.E., 2007. Discrete element method for modelling solid and p articulate materials. Int. J. Numer. Methods Eng. 70, 379–404.

Teran, J., Sifakis, E., Blemker, S.S., Thow-Hing, V.N., Lau, C., Fedkiw, R., 2005. Creating and simulating skeletal muscle from the visible human data set. IEEE Trans. Vis. Comput. Graph. 11, 317–328.

Trotter, J.A., 2002. Structure-function considerations of muscle-tendon junctions. Comp. Biochem. Physiol. 133, 1127–1133.

Trotter, J.A., Hsi, K., Samora, A., Wofsy, C., 1985. A morphometric analysis of the muscle-tendon junction. Anat. Rec. 213, 26–32.

Turrina, A., Martínez-González, M.A., Stecco, C., 2013. The muscular force transmission system: role of the intramuscular connective tissue. J. Bodyw. Mov. Ther. 17, 95–102.

Uchiyama, Y., Miyazaki, S., Tamaki, T., Shimpuku, E., Handa, A., Omi, H., Mochida, J., 2011. Clinical results of a surgical technique using endobuttons for complete tendon tear of pectoralis major muscle: report of five cases. Sport. Med. Arthrosc. Rehabil. Ther. Technol. 3, 20.

Untaroiu, C., Darvish, K., Crandall, J., Deng, B., Wang, J.T., 2005. Characterization of the lower limb soft tissues in pedestrian finite element models. Proceedings of the 19th International Technical Conference on the Enhanced Safety of Vehicles (ESV).

Wang, J.H.-C., 2006. Mechanobiology of tendon. J. Biomech. 39, 1563–1582.

Weiss, J.A., Makerc, B.N., Govindjeed, S., 1996. Finite element implementation of incompressible, transversely isotropic hyperelasticity. Comput. Methods Appl. Mech. Eng. 135, 107–128.

Yucesoy, C.A., F, B.H., Huijing, P.A., Grootenboer, H.J., 2002. Three-dimensional finite element modeling of skeletal muscle using a two-domain approach: linked fiber-matrix mesh model. J. Biomech. 35, 1253–1262.

Zhao, H., Wu, Y.-N., Hwang, M., Ren, Y., Gao, F., Gaebler-Spira, D., Zhang, L.-Q., 2011. Changes of calf muscle-tendon biomechanical properties induced by passive-stretching and active-movement training in children with cerebral palsy. J. Appl. Physiol. 111, 435–442.